Published in final edited form as:

Lab Chip. 2019 January 15; 19(2): 306–315. doi:10.1039/c8lc00825f.

Fabrication of Composite Microfluidic Devices for Local Control of Oxygen Tension in Cell Cultures

Yandong Gao[*,1], **Gulnaz Stybayeva**[1], **Alexander Revzin**[*,1]

[1]Department of Physiology and Biomedical Engineering, Mayo Clinic, Rochester, MN, 55901

Abstract

Oxygen tension is a central component of cellular microenvironment and can serve as a trigger for changes in cell phenotype and function. There is a strong need to precisely control and modulate oxygen tension in cell culture systems in order to more accurately model physiology and pathophysiology observed *in vivo*. The objective of this paper was to develop a simple, yet effective strategy for local control of oxygen tension in microfluidic cell cultures. Our strategy relied on fabrication of microfluidic devices using oxygen-permeable and impermeable materials. This composite device was designed so as to incorporate regions of gas permeability into the roof of the cell culture chamber and was outfitted with a reservoir for the oxygen-consuming chemical, pyrogallol. When assembled and filled with pyrogallol, this device allowed for oxygen depletion to occur within a specific region of the microfluidic culture chamber. The geometry and dimensions of the hypoxic region inside a microfluidic chamber were controlled by features fabricated into the oxygen-impermeable layer. Oxygen tension as low as 0.5% could be achieved using this strategy. To prove the utility of this device, we demonstrated that hypoxia induced anaerobic metabolism in a group of liver cancer cells, and that neighboring cancer cells residing under normoxic conditions upregulated expression of transporters for taking up lactate – a product of anaerobic respiration. The microfluidic devices described here may be broadly applicable for mimicking multiple physiological scenarios where oxygen tension varies on the length scale of tens of micrometers including cancer microenvironment, liver zonation, and luminal microenvironment of the gut.

Keywords

microfluidic; oxygenation; hypoxia; cell culture; cancer

1. Introduction

Oxygen tension varies drastically in a location-specific manner in a number of tissues/organs [1]. In the liver, for example, oxygen varies along the axis extending from the portal to central vein with partial pressure of O_2 (pO_2) at 60–65mm Hg (~8%) in the periportal region and 30–35 mm Hg (~4%) in the pericentral region[2]. This leads to liver zonation and functional differences in hepatocytes residing under different levels of oxygen. Hypoxia is

[*]Corresponding authors: Yandong Gao Ph.D. gao.yandong@mayo.edu, Alexander Revzin Ph.D. revzin.alexander@mayo.edu.

also an important feature of tumor microenvironment and is thought to induce cancer cells to become more aggressive and more resistant to anticancer drugs[3, 4].

There is significant interest in mimicking physiological oxygen tension in vitro, however, standard approaches control oxygen tension globally, for example, by using specialized incubators or hypoxic chambers[5]. In this regard, microfluidic systems hold significant promise for better, more local control of oxygen tension. In fact, a number of studies have reported on controlling oxygen concentration or oxygen gradients in microfluidic devices[6, 7]. One of the early designs was described by Eddington et al. who proposed a multi-layer device containing a gas permeable polydimethylsiloxane (PDMS) membrane that could be used to deliver a well-defined concentration of oxygen or another gas to cells that were located either on top of or underneath the membrane [8, 9]. This approach has been very popular for creating oxygen gradients of different shapes and has been used for culturing bacterial and mammalian cells[10–13]. There are, however, certain complexities associated with using such devices for controlling oxygen tension. First, there is a need for gas cylinders and gas mixers/flow controllers – which makes the system somewhat complicated. Second, existing strategies offer limited control over the shape and location of the oxygen depletion zone within a given device. The first shortcoming can be addressed by utilizing oxygen scavengers in microfluidic devices. For example, an alkaline solution of pyrogallol (PYR) was introduced into the top layer (or side channels) of a microfluidic device resulting in oxygen depletion in the neighboring cell culture chamber[14–17]. The use of an oxygen-absorbing chemical instead of purge gas simplifies the experiment set up around the microfluidic device significantly, albeit at the expense of fine control over the oxygen level and gas composition. The second shortcoming, the inability to precisely control a shape of the hypoxic region or oxygen profiles in the radial direction, has not been addressed to the best of our knowledge.

The goal of this paper was to design a new device fabrication strategy to enable local control of oxygen tension in microfluidic cell cultures. To achieve this, we developed a microfabrication strategy that combines the use of gas-permeable PDMS, a standard polymer used for soft lithography, with NOA81 – a photocurable gas-impermeable polymer. NOA81 is transparent and biocompatible, but more importantly, this material can be replica molded to fabricate features of micrometer-scale resolution[18–20]. In this paper, we fabricated features (openings) of defined geometries within NOA81 membranes and then incorporated these membranes into traditional PDMS-based microfluidic devices. When combined with the oxygen-consuming chemical (PYR) and ambient air, such hybrid devices allowed us to establish hypoxic zones of precise dimensions and geometry inside microfluidic cell culture chambers. We envision that this novel microfabrication strategy may enhance the ability to manipulate cellular microenvironment and may be used to model the effects of oxygen tension on biological processes and diseases.

2. MATERIALS AND METHODS

2.1 Materials

Negative photoresists (SU8–2005 and SU8–2100) along with the developer were purchased from MicroChem (Newton, MA). Polydimethylsiloxane (PDMS, Sylgard 184) was

purchased from Dow Corning (Midland, MI). Glass slides and Pyrex Cloning cylinders (10mm × 10mm) were purchased from Fisher Scientific (Pittsburgh, PA). Glass coverslips (No.1, 24×60mm) were obtained from VWR (West Chester, PA). The photomasks for microfabrication were designed in AutoCAD and printed by CAD/Art Services (Bandon, OR). Tygon microbore tubing and PVC clear vinyl tubing were obtained from Cole-Parmer (Vernon Hills, IL). The oxygen sensing dye Pt(II) meso-tetrakis(pentafluorophenyl)porphine (PtTFPP) was obtained from Frontier Scientific Inc. (Logan, Utah). Toluene, 1× phosphate-buffered saline (PBS) without calcium and magnesium, Dulbecco's Modified Eagle's Medium (DMEM), Minimum Essential Media (MEM), pyrogallol (PYR), NaOH, and collagen were purchased from Sigma-Aldrich (St. Louis, MO). Pimonidazole (PMDZ) HCl and its antibody were obtained as a kit from Hypoxyprobe Inc (Burlington MA). Penicillin, streptomycin, Trypsin-EDTA, sodium lactate, mouse-anti-monocarboxylate transporter 1 (mouse-anti-MCT1), rabbit-anti- monocarboxylate transporter 4 (rabbit-anti-MCT4), DAPI, donkey-anti-rabbit Alexa Fluor® 488, donkey-anti-mouse Alexa Fluor® 546, and Alexa Fluor™ Phalloidin were obtained from Thermofisher (Waltham, MA).

2.2 Design and fabrication of NOA81 and PDMS layers of composite microfluidic devices

A typical microfluidic device (see Fig. 1) was composed of microstructured membranes of gas-permeable PDMS and impermeable NOA. While several device geometries were implemented throughout this study, the fabrication process was similar in all cases. This process will be explained based on the device with a circular hypoxic region shown in Fig. 1a. PDMS and NOA layers were fabricated separately and then assembled into a composite microfluidic device.

Fabrication of PDMS proceeded according to well established protocols. Briefly, SU-8 2100 was spin-coated at the speed of 3000 rpm onto a 4" silicon wafer to create a 100 μm thick layer. This photoresist layer was soft-baked at 65°C for 5min and 95°C for 20min and then exposed to UV light (UV-KUB 3, KLOE, Montpellier, France) through a plastic photomask (CAD/Art Services, Bandon, USA). Exposure lasted for 5 sec at an intensity of 45mW/cm^2. Post exposure baking was carried out at 65°C for 5min and 95°C for 10min on a hot plate and was followed by a 3 min development step. Once the SU-8 pattern was ready, a prepolymer of PDMS (Sylgard 184, Dow Corning, MI) was mixed with a curing agent at a 10:1 ratio and poured onto a wafer. After degassing for 1 h, liquid PDMS was cured for 2 h in a convection oven (Thermofisher, Waltham, MA) at 80°C. The crosslinked PDMS membrane was carefully peeled off the master. A sharp metal puncher (6mm in diameter) was used to make inlet/outlet holes in the layer.

Fabrication of microstructured NOA membranes proceeded in a manner similar to that described for molding of PDMS above; however, instead of SU-8 on silicon wafers, PDMS was used as a template/master for molding NOA. Fig. S1(a-d) shows the steps involved in fabrication of the PDMS mold for devices with circular hypoxic regions described in Fig.1. First, SU-8 2100 photoresist was spun at 1800 rpm onto a silicon wafer. This photoresist layer was then soft baked as described in the paragraph above, exposed to UV light through a photomask for 7 sec, and developed to create SU8 features with 150 μm height (see Fig. S1a). Subsequently, a second SU-8 layer was spun onto the same wafer at a speed of 1800

rpm, aligned with existing SU-8 structures using a second photomask, exposed to UV light, and developed. The resultant SU-8 pattern (see Fig. S1b) was used as a template for molding a PDMS membrane (see Fig.S1c). This molding process was identical to that described in the previous paragraph and resulted in the PDMS membrane shown in Fig. S1d.

To mold NOA81, ~2ml of liquid prepolymer were spread on the PDMS master (Fig. S1e). Care was taken to aspirate bubbles in the prepolymer layer using a pipette. Subsequently, the liquid NOA layer was sandwiched between the PDMS membrane on the bottom and a PDMS-coated glass slide on the top. A 250g lead ring weight was placed on top of this construct in order to squeeze out NOA prepolymer and ensure that the PDMS-covered glass slide was resting on top of the tallest PDMS structure in the bottom membrane (see Fig. S1f). The area where top and bottom PDMS layers met would later become the through hole in the NOA membrane. Exposure to UV ($2mW/cm^2$) for 5 min was used to convert liquid NOA81 prepolymer into a membrane. When peeled off from the PDMS master, the NOA membrane (Fig. 1c) contained a circular through hole corresponding in size to the hypoxic region as well as air side channel (its function will be explained in section 3.1).

2.3 Assembly of composite microfluidic devices

Assembly of PDMS and NOA membranes into a microfluidic device occurred according to following steps. A PDMS layer was treated by exposure to oxygen plasma (Harrick Instruments, town, state) for 2 min and then was bonded onto a glass slide. This created channels/chambers for cultivation of cells. Subsequently, the roof of this PDMS layer and the NOA81 layer were treated with oxygen plasma. After filling the PDMS microfluidic chamber with DI water, the NOA layer was aligned under a stereomicroscope and bonded onto the PDMS roof. The presence of water in the microfluidic chambers prevented the PDMS roof from distending and adhering to the glass floor of the microfluidic channel. The PYR reservoir was fabricated by cutting clear PVC tubing (7/8” OD and ½” ID) into 10mm long cylinders. Holes were drilled in these cylinders using a Dremel rotary tool. Tygon microbore tubing was inserted into these holes and bonded using liquid NOA81 as glue. A reservoir for the oxygen scavenger (PYR) PVC was also covered by a piece of glass using the NOA81 as the glue. Fig. S2 shows a photo of an assembled device.

2.4 Fabrication of the oxygen sensing PDMS film

Oxygen sensing films were incorporated into microfluidic devices in order to verify the presence of hypoxic regions. These films were fabricated according to protocols described previously, by incorporating oxygen sensing dye, PtTFPP, into PDMS prepolymer [21]. Briefly, 11.67mg PtTFPP was dissolved in 2mL toluene in a glass container. After intensive vortexing, the solution was filtered through a 0.2 μm filter to remove undissolved particles. Then the solution was mixed with 9.65g PDMS (base and curing agent mixture at a 10:1 ratio). After degassing for 30 min, the mixture was spin-coated on a glass slide for 30 sec at the speed of 800 rpm. The liquid PDMS film was then left in a chemical hood for 4 h to allow for toluene to evaporate and cured in an oven at 80°C overnight. This resulted in approximate 150 μm thick oxygen sensing PDMS layer. For oxygen calibration experiments, a single channel microfluidic channel was placed directly onto PtTFPP-PDMS coated glass.

An IX83 microscope (Olympus Corp, Center Valley, PA) with TRITC filter was used to record fluorescence images.

2.5 Cultivation of cells in microfluidic devices

Both Caco2 and HepG2 cell lines were obtained from ATCC (Manassas, VA). HepG2 cells were cultured in DMEM containing 10% FBS and 1% penicillin/streptomycin at 37°C with 5% CO2. Caco2 cells were cultured in MEM containing 10% FBS and 1% penicillin/streptomycin. Before seeding cells, the microfluidic devices were sterilized under UV light for 1h and then coated with collagen 1 (0.1 mg/ml) for 1h at 37°C in a tissue culture incubator. After washing out the collagen solution, microfluidic channels were filled with culture media for priming devices prior to introduction of cells. HepG2 or Caco2 cells were resuspended in their respective media at a concentration of 2000 cells/μl. Media in reservoirs of microfluidic chambers was then replaced with 10 to 30 μl of cell suspension. Flow rate was adjusted by controlling liquid head at the inlet and outlet media reservoirs. Once a preferred flow rate (~50μm/s) was obtained, microfluidic devices were placed in a tissue culture incubator with 21% oxygen and 5% CO_2 for 3h at 37°C to allow cells to attach to collagen-coated substrates.

To induce hypoxia, 2ml (10mg/ml) PYR and 0.2ml 1N NaOH were injected into the PYR reservoir. The tubing leading into and out of the PYR reservoir was clamped, and devices were then placed into tissue culture incubator in order to ensure that hypoxia was carried out under normal physiological conditions. Hypoxic conditions were maintained between 2h and 6h depending on experimental goals. For evaluating hypoxia in cells, PMDZ was dissolved in cell culture media at a concentration of 2mg/ml and was introduced into microfluidic devices containing cells.

2.7 Immunofluorescent staining of cells under hypoxic and normoxic conditions in microfluidic devices.

For immunostaining, cells in microfluidic devices were washed with 1× PBS for 3 min and then fixed with 4% PFA and 0.2% Triton-X100 for 30 min at room temperature. We should note that the oxygen scavenger was present in the oxygen control layer to ensure that hypoxic conditions were maintained up to the end of the fixation protocol. After washing, cells were blocked with 1% BSA overnight at 4°C. The primary antibodies were then added and devices were left in the refrigerator overnight at 4°C. After washing, cells were incubated with secondary antibodies for 1h at room temperature. Concentration of the primary antibodies was as follows: anti-PMDZ (3 μg/ml), anti-MCT1(4 μg/ml) and anti-MCT4(4 μg/ml). For actin staining, phalloidin was diluted at a 1:20 ratio in the secondary antibodies according to the manufacturer's instructions. Finally, devices were filled with 1× PBS and stored at 4°C prior to imaging.

The PYR reservoir and NOA81 layer were carefully removed before imaging. An Olympus IX83 microscope equipped with DAPI, FITC, TRITC and Cy5 filter was used for imaging. The fluorescence intensities were calculated by NIH ImageJ.

3. RESULTS

3.1 Local control of geometry and location of hypoxic zone using NOA oxygen control mask

To control the location and geometry of a hypoxic region, we integrated a microfabricated gas-impermeable layer into a PDMS-based microfluidic device. This gas-impermeable layer included holes and channels with different sizes and shapes which defined different oxygen boundary conditions of microfluidic cell culture chambers. We termed the NOA layer "oxygen control mask" because this membrane serves the purpose similar to that of a photolithography mask, but instead of transmission of light, it helps control diffusion of oxygen. Similar to problems associated with divergence of light during non-contact UV exposure, there are challenges with confining hypoxic regions to features defined in an NOA membrane. To address these challenges, we incorporated channels for delivery of air next to regions of hypoxia. This technological solution is highlighted in Fig.1a which shows a device used to create circular hypoxic region inside a microfluidic culture chamber. As seen from Fig.1b, the oxygen scavenger (PYR) is in direct contact with the gas-permeable PDMS layer creating a cylindrical oxygen depletion zone in the culture media. Importantly, this oxygen-depletion region is flanked by channels containing ambient air. The purpose of these channels is to prevent expansion of hypoxic regions over time.

Fig. 1(d,e) show COMSOL simulation of oxygen distribution inside the PDMS roof and media in the cell culture chamber, respectively. The oxygen concentration inside the media depends on oxygen diffusion, the shape and location of the window within the NOA81 membrane and the nearby air access channels. The importance of this design is highlighted by a panel of images in Fig. 2(a-d), which show expansion of hypoxic regions in a device where air channels are absent as the oxygen is continuously depleted. The reader should note that oxygen quenches PtTFPP fluorescence and that a high fluorescence signal demarcates a hypoxic zone. In contrast, when the device contains air channels for buffering oxygen levels, the diameter of the circular hypoxic region remains constant over the course of 1.5h and similar to the circular opening in an NOA membrane (see images in Fig.2(e-h). It is worth noting that active delivery of air is unnecessary to stabilize hypoxic regions because of the high content and fast diffusion of oxygen in air (see supplementary section S1 for the data); instead air access ports/channels were simply left open to the ambient environment.

We should also note that this fabrication and device design strategy allows us to create hypoxic regions of arbitrary shapes and dimensions. As an example, Fig. 2 (i-l) show half-moon and star-shaped hypoxic regions created in microfluidic devices. There are a number of papers describing control of oxygen tension in microfluidic chamber; however, to the best of our knowledge, the results presented in Fig. 2 are some of the first describing confinement and maintenance of a hypoxic zone in a microfluidic device.

3.2 Controlling oxygen levels in microfluidic co-culture devices

Having established that our composite microfluidic devices may be used for local control of oxygen tension, we wanted to utilize this concept to impose local hypoxia in microfluidic cell cultures. Our lab has been interested in microfluidic co-cultures where two groups of

cells reside in close proximity and exchange paracrine signals [22–26]. In the present paper, we incorporated the ability to control oxygen into a microfluidic co-culture platform. As shown in Fig. 3, a PDMS-based microfluidic device with two culture chambers interconnected by grooves was modified to include an NOA layer containing a rectangular through-hole and an air access port (see Fig. 3a). Detailed dimensions of microfluidic co-culture devices are provided in Fig. S4. The NOA layer was mounted on top of PDMS channels. In addition, this composite microfluidic device was outfitted with a reservoir for an oxygen scavenging chemical (PYR) [14–16]. When perfused through this reservoir, the alkaline PYR solution came in direct contact with regions of PDMS membrane residing beneath the rectangular opening in the NOA layer. As a result, the microenvironment beneath the PDMS membrane became hypoxic. The neighboring culture chamber remained normoxic, in part because it was distant from the oxygen depletion zone but also because of oxygen diffusing through the PDMS roof. Fig. 3b describes the concept of oxygen consumption in one chamber being counterbalanced by a supply of oxygen with ambient air in the neighboring cell culture chamber. An image of the device is provided in Fig. 3c. The advantage of using PYR is that devices don't require external connections or gas sources. Because of this, a device can be placed into a standard 100 mm Petri dish (see Fig. 3c) and moved from one experimental station to the next (e.g. incubator, microscope, tissue culture hood).

In order to characterize oxygen concentration, a PDMS layer impregnated with oxygen-sensitive fluorophore, PtTFPP, was bound to the floor of a microfluidic device. A mixture of PYR and NaOH was added into the reservoir creating alkaline conditions for oxygen consumption. The device was then mounted onto the stage of a fluorescence microscope for time-lapse imaging. Fluorescence signal (indication of hypoxia) became detectable ~5 min after injection of PYR and stabilized 25 min after injection. To determine stability of hypoxic zone over time we carried out time-lapse fluorescence imaging as shown in Fig. 4a. Movies S1 and S2 show shorter term (45 min) and longer term (24h) stability of the rectangular hypoxic zone in a co-culture system. These images and the supplementary movies highlight the fact that hypoxia is established rapidly and can be maintained for up to 9 h. It is likely that oxygen scavenging ability of PYR is depleted after 9h which in turn causes oxygen levels to rise (increase in fluorescence in Movie S2). This suggests that PYR solution may need to be exchanged every 9h to maintain hypoxia in the current format of the device. As an alternative to periodic exchange, PYR may be perfused to ensure constant supply.

Fluorescence microscopy in a two-chamber microfluidic device (see Fig. 4) highlights the fact that one chamber is hypoxic (red fluorescence) while the neighboring chamber is normoxic. Importantly, fluorescence signal could be correlated to oxygen tension with the aid of a calibration curve. In a calibration experiment, microfluidic devices were infused with different oxygen-nitrogen mixtures ranging from 0% to 20% oxygen. Fig. S5 shows fluorescence response to different concentrations of oxygen. Using this calibration curve, we converted raw fluorescence intensity vs. position data shown in Fig. 4d into oxygen concentration vs. position plot shown in Fig. 4e. As seen from the latter plot, oxygen tension was ~ 0.5% in the majority (~60%) of the hypoxic chamber and ~15% in the normoxic chamber.

The oxygen profile in Fig. 4e highlights a gradient in oxygen tension between hypoxic and normoxic chambers. This gradient is affected by the thickness of the gas permeable PDMS layer in the roof of the device (300 μm). Our modeling (data not shown) reveals that the transition between low and normal oxygen zones may be made sharper by using thinner PDMS membranes (<150 μm).

3.3 Demonstrating local hypoxia in microfluidic device.

Upon fabricating microfluidic co-culture devices and characterizing oxygen profile in these devices, we carried out experiments to co-culture normoxic and hypoxic cells. In these experiments, we used pimonidazole (PMDZ) – an oxygen sensitive probe that is activated at low oxygen tension (<1.3% or 10 mmHg) [27]. Exposure to low oxygen creates reactive intermediates of PMDZ which form adducts to proteins and can be detected using immunofluorescent staining. One should note that this approach is semi-quantitative in that fluorescence intensity of staining is not directly proportional to oxygen concentration. This approach can, however, indicate hypoxia in cells.

For proof of concept experiments, we cultured colon cancer cells (Caco2) in the composite microfluidic devices. Oxygen depletion experiments commenced on day 3 and hypoxia probe PMDZ was added into culture media shortly thereafter. After 2 h of hypoxic treatment, cells were fixed and stained for PMDZ adducts as well as for the cytoskeletal marker (actin). As seen from Fig. 5 (a,b), fluorescence intensity due to PMDZ adducts was high in the hypoxic chamber and considerably lower in the normoxic chamber, pointing to the possibility of imposing local hypoxia in a microfluidic chamber. The hypoxic region in cells corresponded with low oxygen region measured using oxygen sensing film in Fig. 4e.

In another proof of concept experiment we wanted to demonstrate that hypoxia may be imposed locally within a monolayer of epithelial cells. In this experiment, Caco2 cells were cultured in the device of the type shown in Fig. 1a containing a circular oxygen depletion region with diameter of 1 mm. After cultivation in such a device for 6h, Caco2 cells were stained for hypoxia using PMDZ and for actin using phalloidin. Fig.5c demonstrates the presence of circular hypoxic region surrounded by normoxic Caco2 cells. The dimensions of hypoxic region in cell monolayer corresponded to the dimensions of the circular region in the oxygen control mask.

3.4 Metabolic adaptations due to communication between hypoxic and normoxic cancer cells in microfluidic co-culture devices

In the next set of experiments, we wanted to provide an example of interactions between hypoxic and normoxic cell compartments. Cancer cells are notorious for reprogramming their metabolism to respond and adapt to the local microenvironment[28 29]. One example of metabolic adaption is related to co-localization of hypoxic and normoxic regions within the tumor and subsequent interactions between cells respiring aerobically and anaerobically [30]. Specifically, studies have shown that cancer cells residing in hypoxic microenvironment upregulate expression of monocarboxylate transporter 4 (MCT4) responsible for efflux of lactate, a byproduct of anaerobic respiration. Interestingly, cancer cells in the neighboring normoxic regions have been shown to upregulate expression of monocarboxylate transporter

4 (MCT1) – a transporter responsible for influx of lactate. Recent studies have shown that lactate may be an important signal triggering angiogenesis in the tumor microenvironment. Furthermore, this molecule may also be used as a substrate for energy metabolism. Interestingly, studies suggested a symbiotic relationship between normoxic and hypoxic cells with the former utilizing lactate as energy source and thereby making glucose available for consumption by hypoxic cells[31, 32]. A schematic of this model is shown in Fig. S6. Blocking of MCT1 in normoxic regions of the tumors decreased availability of glucose and led to cell death in hypoxic regions of the tumor [31, 32].

To demonstrate utility of a microfluidic device with local control of oxygen tension, we created co-cultures of normoxic and hypoxic liver cancer cells (HepG2). Three days after seeding cells, hypoxia was induced in one compartment of the co-culture device using an alkaline PYR solution as described above, after which devices were placed into a tissue culture incubator for 6 h. Immunofluorescent staining shown in Fig. 6(a-e) revealed that HepG2 cells under hypoxic conditions upregulated expression of MCT4 and downregulated MCT1, conversely cells in the normoxic regions had a lower expression of MCT4. A plot of the ratio of MCT4 to MCT1 fluorescence intensity along the axis of the oxygen gradient (see Fig. 6f) illustrates that cancer cells regulated expression of lactate efflux and influx transporters according to the gradient. The experiment detailed in Fig. 6 demonstrates how imposition of local hypoxia in microfluidic devices recapitulates observations made previously using considerably more complicated experimental approaches.

4. CONCLUSIONS

Oxygen tension varies dramatically in spatial, temporal, and organ-specific manner in the human body. Microfluidic devices have emerged as promising tools for controlling oxygen concentration on the microscale. Our paper adds to the repertoire of such devices by demonstrating, for the first time, precise and local control of the shape, dimension, and location of the oxygen depletion zone. This ability is enabled by the new microfabrication approach that integrates gas-impermeable NOA membranes into gas-permeable PDMS-based devices. In addition, we made use of supplemental air channels to ensure that the oxygen depletion zone is contained to the geometry defined within the NOA layer. These technological advances allowed us to create circular, star-shaped, or half-moon shaped regions of low oxygen. To demonstrate biological utility of this fabrication strategy, we created microfluidic co-cultures and demonstrated that imposition of hypoxia in one cell compartment led to metabolic adaptation in the other cell compartment. Importantly, devices described here are simple to fabricate using standard soft lithography approaches. In addition, they are simple to operate and handle– not requiring lines or pumps for delivery of gases or oxygen scavengers. Moving forward, we envision using these devices for mimicking physiological scenarios where oxygen heterogeneity or gradients are particularly important, for example, liver zonation, gut lumen, and cancer microenvironment. These devices may also be combined with biosensors for monitoring cellular responses to local changes in oxygen tension.

Supplementary Material

Refer to Web version on PubMed Central for supplementary material.

Acknowledgement:

This study was supported in part by a grant from NIH (R21NS95325).

Reference:

1. Carreau A, El Hafny-Rahbi B, Matejuk A, Grillon C and Kieda C, J Cell Mol Med, 2011, 15, 1239–1253. [PubMed: 21251211]
2. Gebhardt R and Matz-Soja M, World journal of gastroenterology, 2014, 20, 8491–8504. [PubMed: 25024605]
3. Hockel M and Vaupel P, Journal of the National Cancer Institute, 2001, 93, 266–276. [PubMed: 11181773]
4. Brown JM and Wilson WR, Nature reviews. Cancer, 2004, 4, 437–447. [PubMed: 15170446]
5. Byrne MB, Leslie MT, Gaskins HR and Kenis PJA, Trends Biotechnol, 2014, 32, 556–563. [PubMed: 25282035]
6. Brennan MD, Rexius-Hall ML, Elgass LJ and Eddington DT, Lab on a chip, 2014, 14, 4305–4318. [PubMed: 25251498]
7. Oomen PE, Skolimowski MD and Verpoorte E, Lab on a chip, 2016, 16, 3394–3414. [PubMed: 27492338]
8. Lo JF, Sinkala E and Eddington DT, Lab on a chip, 2010, 10, 2394–2401. [PubMed: 20559583]
9. Oppegard SC, Nam KH, Carr JR, Skaalure SC and Eddington DT, Plos One, 2009, 4.
10. Adler M, Polinkovsky M, Gutierrez E and Groisman A, Lab on a chip, 2010, 10, 388–391. [PubMed: 20091013]
11. Lam RHW, Kim MC and Thorsen T, Analytical chemistry, 2009, 81, 5918–5924. [PubMed: 19601655]
12. Polinkovsky M, Gutierrez E, Levchenko A and Groisman A, Lab on a chip, 2009, 9, 1073–1084. [PubMed: 19350089]
13. Takano A, Tanaka M and Futai N, Biomicrofluidics, 2014, 8, 061101. [PubMed: 25553177]
14. Chang CW, Cheng YJ, Tu M, Chen YH, Peng CC, Liao WH and Tung YC, Lab on a chip, 2014, 14, 3762–3772. [PubMed: 25096368]
15. Chen YA, King AD, Shih HC, Peng CC, Wu CY, Liao WH and Tung YC, Lab on a chip, 2011, 11, 3626–3633. [PubMed: 21915399]
16. Peng CC, Liao WH, Chen YH, Wu CY and Tung YC, Lab on a chip, 2013, 13, 3239–3245. [PubMed: 23784347]
17. Wang L, Liu WM, Wang YL, Wang JC, Tu Q, Liu R and Wang JY, Lab on a chip, 2013, 13, 695–705. [PubMed: 23254684]
18. Alvankarian J and Majlis BY, J Micromech Microeng, 2012, 22.
19. Bartolo D, Degre G, Nghe P and Studer V, Lab on a chip, 2008, 8, 274–279. [PubMed: 18231666]
20. Levache B, Azioune A, Bourrel M, Studer V and Bartolo D, Lab on a chip, 2012, 12, 3028–3031. [PubMed: 22855124]
21. Thomas PC, Halter M, Tona A, Raghavan SR, Plant AL and Forry SP, Analytical chemistry, 2009, 81, 9239–9246. [PubMed: 19860390]
22. Gao YD, Majumdar D, Jovanovic B, Shaifer C, Lin PC, Zijlstra A, Webb DJ and Li DY, Biomedical microdevices, 2011, 13, 539–548. [PubMed: 21424383]
23. Majumdar D, Gao YD, Li DY and Webb DJ, J Neurosci Meth, 2011, 196, 38–44.
24. Shi MJ, Majumdar D, Gao YD, Brewer BM, Goodwin CR, McLean JA, Lib D and Webb DJ, Lab on a chip, 2013, 13, 3008–3021. [PubMed: 23736663]

25. Patel D, Gao YD, Son K, Siltanen C, Neve RM, Ferrara K and Revzin A, Lab on a chip, 2015, 15, 4614–4624. [PubMed: 26542093]
26. Gao YD, Broussard J, Haque A, Revzin A and Lin T, Microsyst Nanoeng, 2016, 2.
27. Hypoxyprobe, http://www.hypoxyprobe.com/knowledge-center.html, 2017.
28. Martinez-Outschoorn UE, Peiris-Pages M, Pestell RG, Sotgia F and Lisanti MP, Nature Reviews Clinical Oncology, 2017, 14, 11–31.
29. Icard P, Kafara P, Steyaert JM, Schwartz L and Lincet H, Bba-Rev Cancer, 2014, 1846, 216–225.
30. Nakajima EC and Van Houten B, Molecular carcinogenesis, 2013, 52, 329–337. [PubMed: 22228080]
31. Sonveaux P, Copetti T, De Saedeleer CJ, Vegran F, Verrax J, Kennedy KM, Moon EJ, Dhup S, Danhier P, Frerart F, Gallez B, Ribeiro A, Michiels C, Dewhirst MW and Feron O, Plos One, 2012, 7.
32. Kennedy KM, Scarbrough PM, Ribeiro A, Richardson R, Yuan H, Sonveaux P, Landon CD, Chi JT, Pizzo S, Schroeder T and Dewhirst MW, Plos One, 2013, 8.

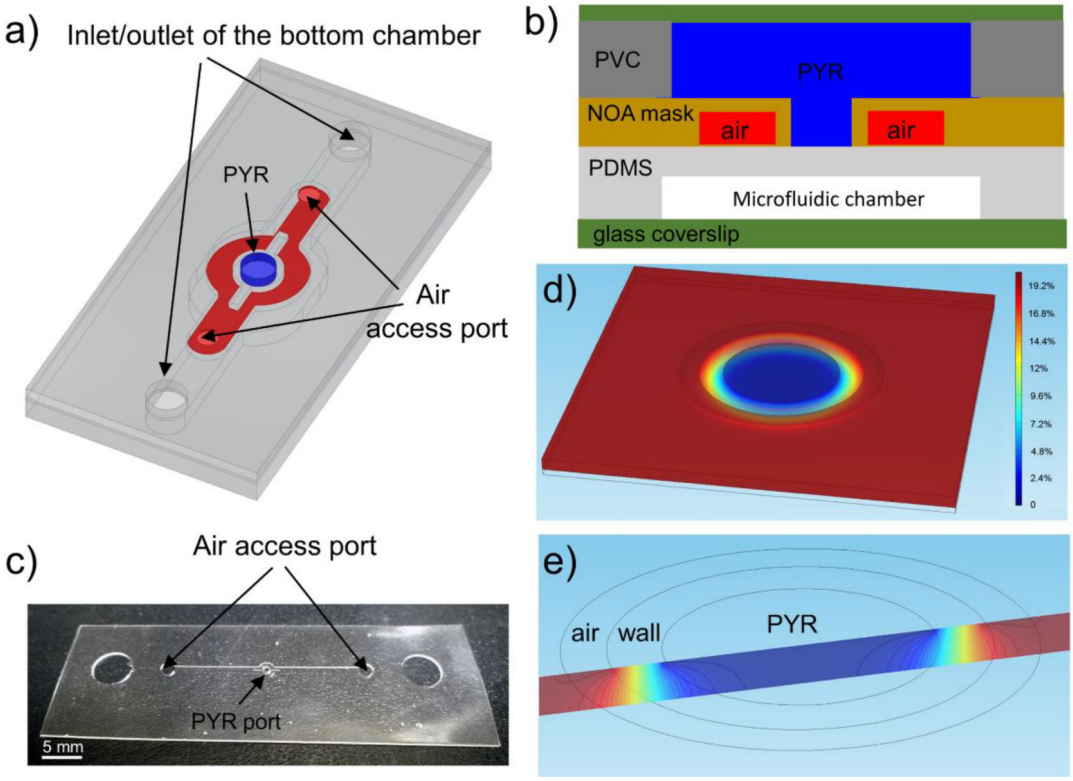

Fig. 1: The design principle of the NOA81 O_2 mask.

a) Layout of a hybrid device used to generate a circular region of hypoxia. (Note: reservoir with oxygen scavenger is not shown). b) Cross-sectional view of the microfluidic device comprised of NOA81 and PDMS (not drawn to scale). Blue and red colors show oxygen scavenging chemical (PYR) and air, respectively. Air channels are used to contain and confine oxygen depletion zone. c) An image of features microfabricated in NOA81 layer and used for defining where oxygen scavenging chemical comes in contact with the underlying PDMS layer. d) COMSOL numerical simulation of the oxygen transport inside the PDMS film. e) A section view of the oxygen distribution on a slice passing the center of the circle.

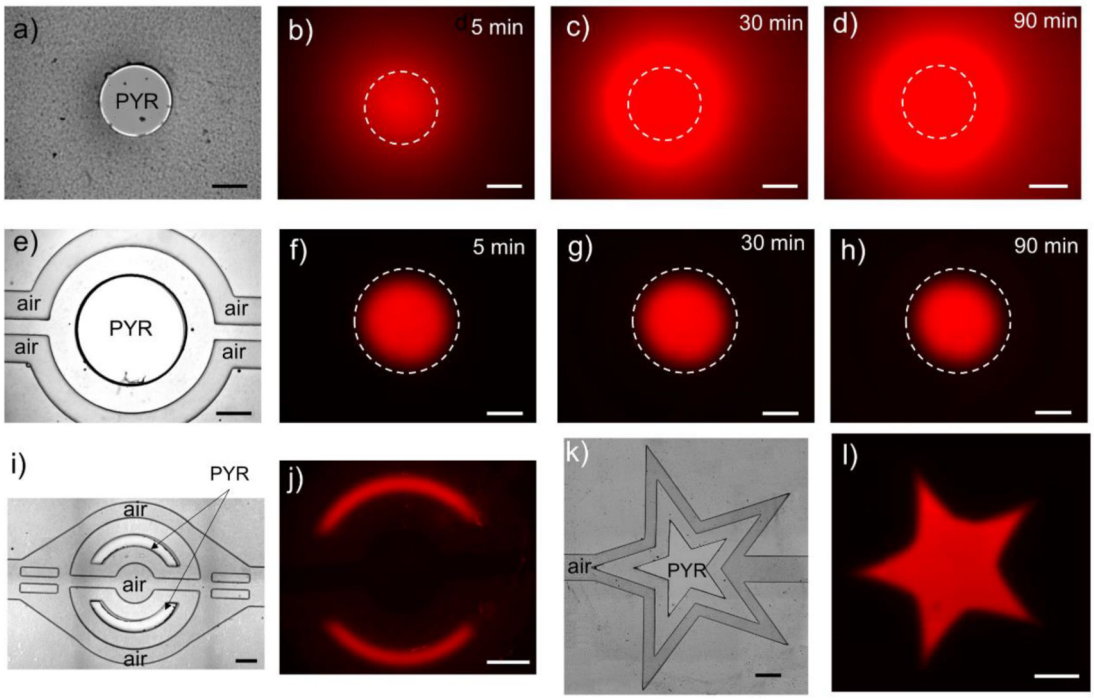

Fig. 2: Arbitrary control of hypoxic regions in hybrid microfluidic devices.

a) A brightfield image of a device where a circular opening in NOA is not flanked by air channels. b-d) Oxygen sensing dye was impregnated into the microfluidic device and was used to monitor hypoxic one over time. As can be seen from these images, without a supply of air from auxiliary channels, hypoxic zone spreads over the course of 1.5 h. e) A brightfield image of a device where circular opening in NOA mask is flanked by the side air channels. f-h) Time-lapse images of oxygen sensing fluorescence dye over the course of 1.5 h. As seen from these images, presence of air supply channel makes hypoxic zone stable. i) A brightfield image of the device used to generate two half-moon hypoxic zones. f) Corresponding fluorescence signal from the same device after 30 min of hypoxia. k) A brightfield image of a device used to generate a star-shaped hypoxic zone. l) Corresponding fluorescence image from the same device after 30min of hypoxia. The scale bars are 500μm in all figures.

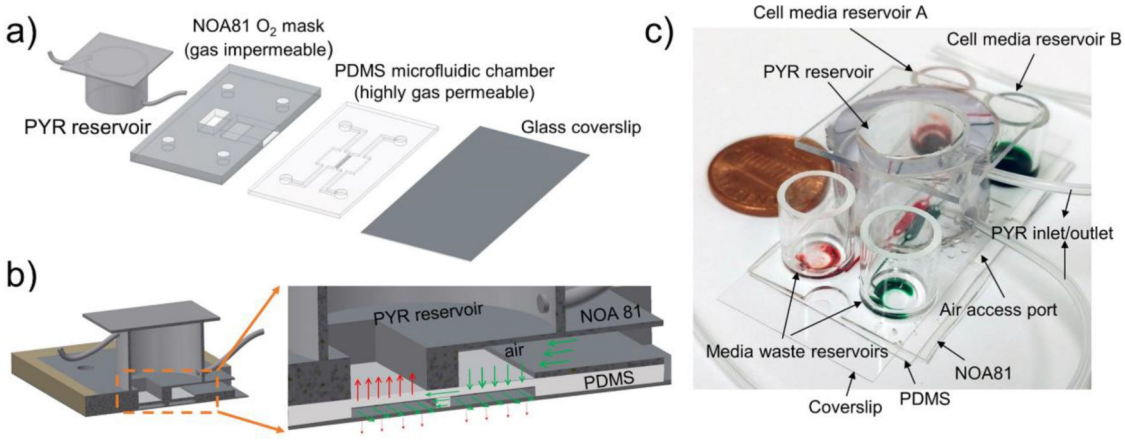

Fig. 3: A two-chamber microfluidic device for inducing hypoxia in cell co-cultures.

a) The device is comprised of a glass slide as a cell culture surface, a PDMS layer containing microfluidic chambers for co-cultivation of two groups of cells, an NOA gas-impermeable layer containing through holes and a reservoir for loading oxygen scavenging chemical. A through hole inside the NOA mask is aligned above the region of PDMS layer containing one of cell culture chambers. When oxygen scavenger, PYR, is loaded into the system it creates hypoxic conditions in one of the cell culture chambers while the neighboring chamber remains normoxic. Communication between groups of normoxic and hypoxic cells occurs via grooves (5×20×100μm, height×width×length, and 30μm spacing) molded into the bottom of the wall separating the two chambers. b) A cross-sectional view showing oxygen transport in the device. Red arrows show depletion of oxygen through a window molded in NOA layer while green arrows show diffusion of oxygen through the air access port. c) An image demonstrating that a device is compact, without gas lines and can be easily transported between different experimental stations. Devices can be loaded with oxygen scavenger PYR and placed into tissue culture incubator to create physiological conditions for cells.

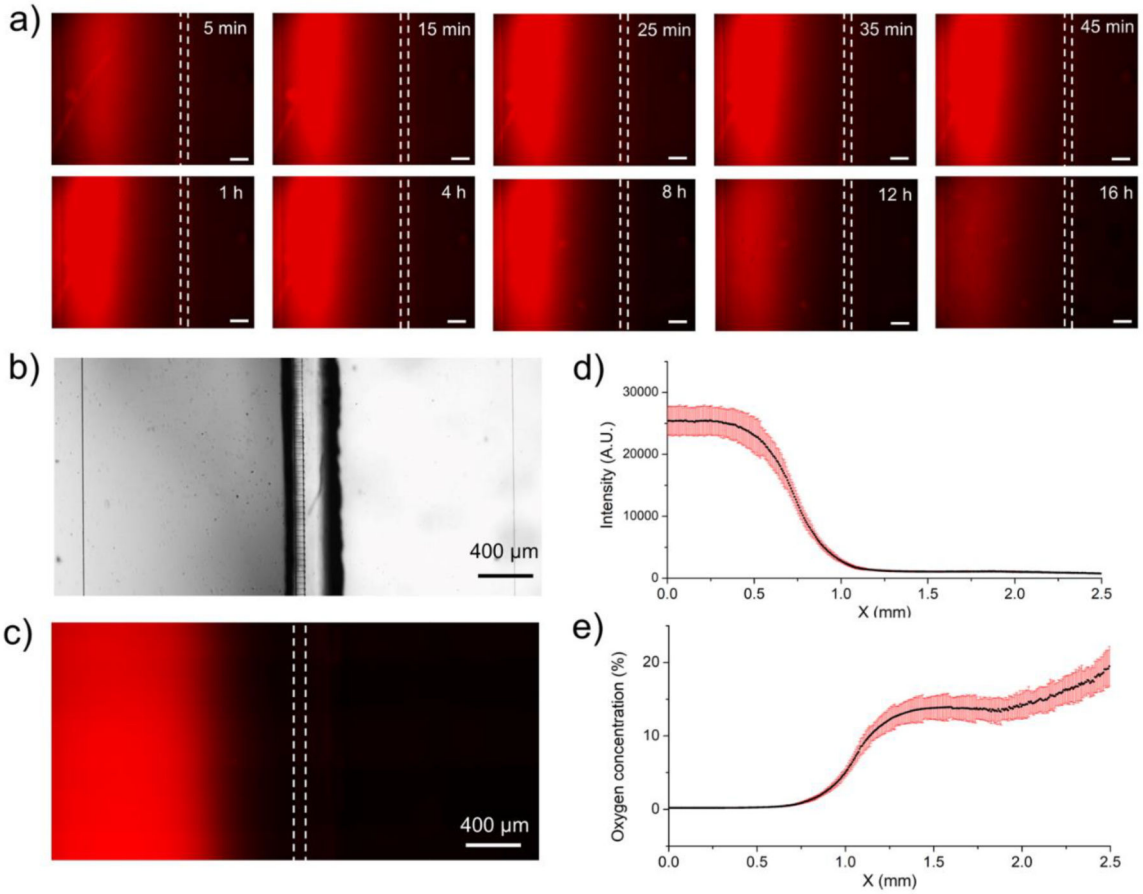

Fig. 4: Characterizing hypoxia in a microfluidic co-culture device.

a) Time-lapse images of oxygen sensing fluorescence dye to show how the hypoxia in left chamber was established in the first 45 minutes and lasted for 16 hours. The scale bars are 200μm in these figures. b) A bright-field image of the two-chamber device. c) Fluorescence intensity as a function of location in a co-culture device. Both images were taken at the same location. High fluorescence signal on the left indicate hypoxia, low fluorescence on the right of the device indicates normoxia. d) Measured fluorescence intensity in x direction. e) Fluorescence intensity was converted into oxygen concentration using a calibration curve (described in Fig. S5).

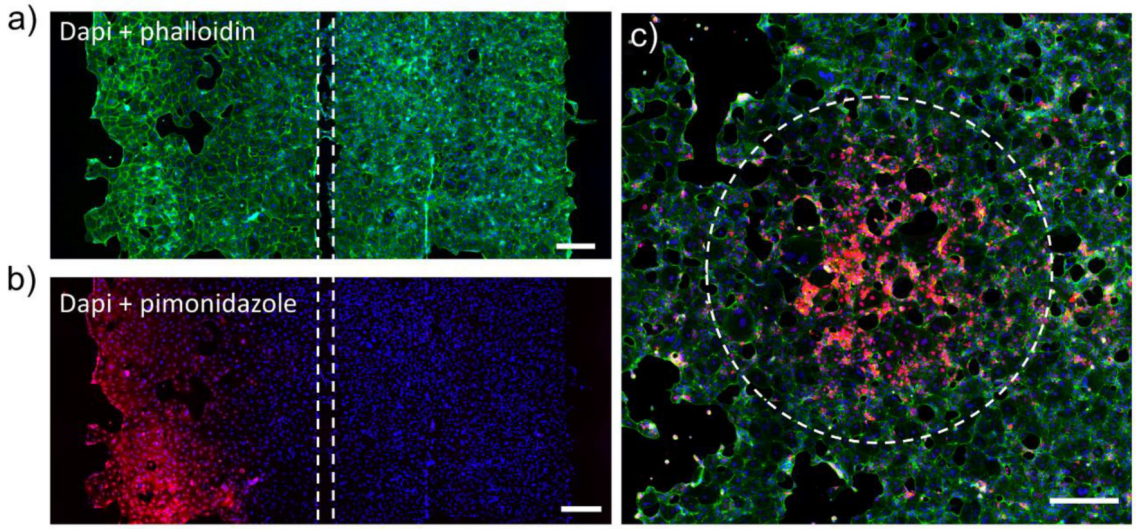

Fig. 5: Effects of local hypoxia on cells in a microfluidic co-culture device.

Hypoxia was induced in the left culture chamber for 2 h, then cells in both chambers were stained with the hypoxic probe. a) Staining for actin (phalloidin -green) and nuclei (Dapi - blue) demonstrating similar cell distribution, density and morphology in both culture chambers. b) Immunofluorescent staining for PMDZ adducts demonstrate that cells in the left chamber were exposed to hypoxic conditions (pO_2 < 10mmHg) while cells in the right chamber remained normoxic. c) Immunofluorescent staining for PMDZ(red), actin (phalloidin -green) and nuclei (Dapi - blue) to show a circular hypoxic pattern. The scale bars are 200μm in all figures.

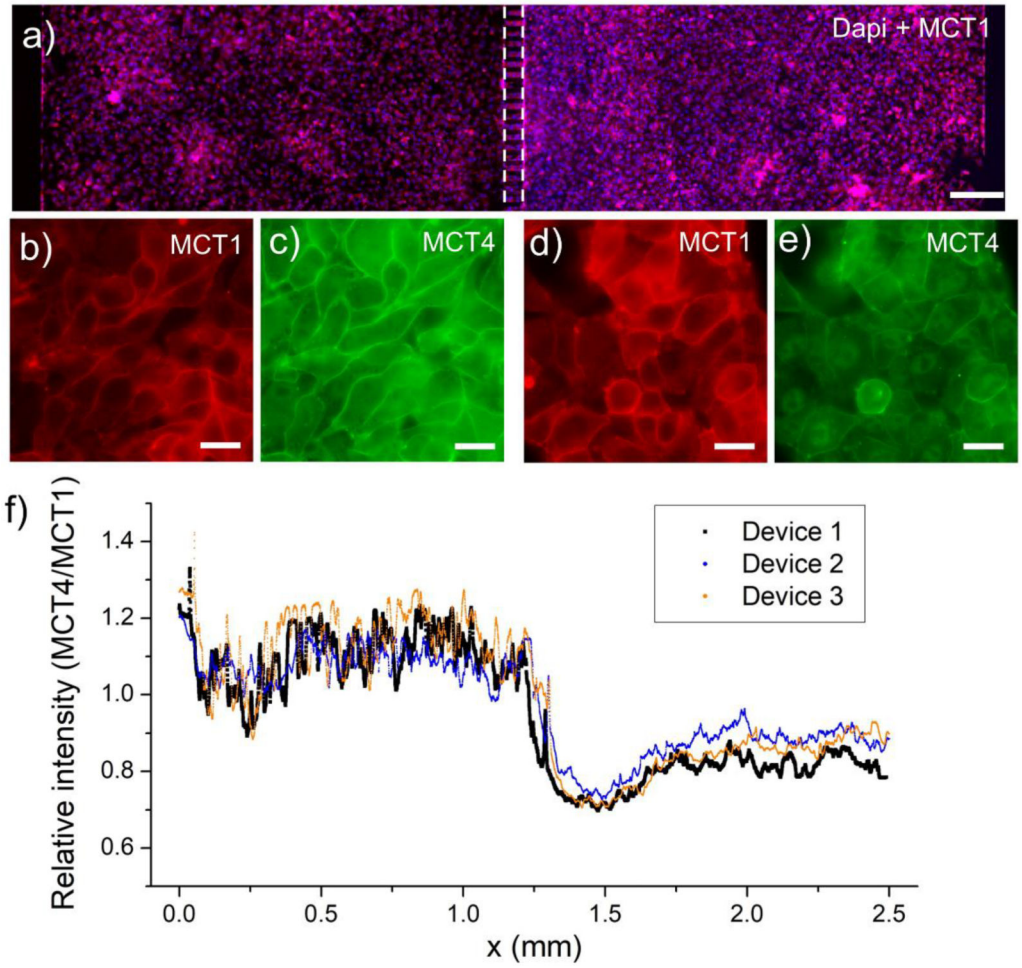

Fig. 6: Metabolic adaptation of liver cancer cells induced by local hypoxia in a microfluidic co-culture device.

a) An immunostaining of MCT1 (red) and Dapi (blue) to show the Caco2 cells in the two chambers. The scale bar is 200μm. b-e) Immunofluorescence staining for lactate efflux (MCT4) and influx (MCT1) transporters in a co-culture device where HepG2 cells in the left chamber are exposed to low oxygen conditions whereas HepG2 cells in the right chamber are under normal oxygen conditions. f) The ratio of MCT4/MCT1 expression across the two chambers demonstrating that lactate efflux transporter (MCT4) is expressed at a higher level in cells exposed to hypoxia. Conversely expression of lactate influx transporter (MCT1) was expressed at a higher level in normoxic cells than in neighboring hypoxic cells